LRP 361/88 November 1988

NUMERICAL SIMULATIONS OF SAWTEETH IN TOKAMAKS

G. Vlad and A. Bondeson

Paper submitted to Nuclear Fusion

NUMERICAL SIMULATIONS OF SAWTEETH IN TOKAMAKS

G. Vlad

Associazione Euratom-ENEA sulla Fusione
Centro Ricerche Energia Frascati
C.P. 65, 00044 Frascati,Rome,Italy

A. Bondeson

Centre de Recherches en Physique des Plasmas
Association Euratom-Confédération Suisse
Ecole Polytechnique Fédérale de Lausanne
21 Av. des Bains, CH-1007 Lausanne,Switzerland

Abstract: Numerical simulations of sawteeth in tokamaks have been carried out using reduced magnetohydrodynamics and a simple transport model. The electron temperature is evolved self-consistently including ohmic heating and a strongly anisotropic thermal conductivity. The character of the sawteeth is found sensitive to the values of the transport coefficients. In particular, the perpendicular viscosity ν must be comparable to, or larger than, the perpendicular heat conductivity $\chi_\perp$ in order for distinct relaxation oscillations to occur. To study the region of high Lundquist number S (up to 10^7), ν and $\chi_\perp$ have been scaled as 1/S, and S has been varied. The influence of the Lundquist number on the sawteeth is strongly affected by modifications of the equilibrium induced by the sawteeth themselves. The collapse time shows a much weaker dependence on S than the expected $S^{1/2}$ scaling, because the deviation of central q away from unity over the sawtooth cycle decreases for increasing S. Furthermore, the resistive instability is turned on quickly because the shear changes from almost zero in the central region to order unity over one resistive layer width. The simulated sawtooth period and collapse time for $S \leq 10^7$ compare favorably with those observed in small and medium size tokamaks.

1. Introduction

Sawtooth oscillations in which the central temperature shows a sudden drop followed by a slow increase until the next drop [1] occur in practically all tokamaks under a variety of experimental conditions. A theoretical model for the sawteeth was proposed by Kadomtsev [2]. In his model, the drop is triggered by the growth of the m=1/n=1 resistive kink mode when the safety factor in the centre q_0 falls below unity. Via a complete resistive reconnection of the helical flux inside the q=1 surface, the deformation relaxes to a symmetrical state with q above unity everywhere and a flattened temperature profile in the central region of the plasma. After such an internal disruption, the temperature and current profiles peak again under the influence of ohmic heating, q_0 again falls below unity and the cycle is repeated. Recent experimental data indicates that the Kadomtsev model is not always applicable and suggests that the central q may be significantly less than unity while the discharge is still sawtoothing [3]. Furthermore, measurements on JET indicate that the growth-time of the instability leading to the drop in central temperature is too short to be connected with a resistive mode [4,5].

The first simulations of sawteeth were performed by Waddell et al. [6], using reduced magnetohydrodynamics (MHD). Sykes and Wesson [7] followed repeated oscillations, assuming Spitzer resistivity $\eta \propto T^{-3/2}$ and using an equation for the temperature evolution that included ohmic heating and perpendicular thermal diffusion. In this model the oscillations were found to decay in time. Denton et al. [8,9] and Bondeson [10] reproduced periodic oscillations by introducing a large thermal conductivity along the field-lines.

All computations carried out so far have been made with plasma parameters far from those characteristic of current experiments. The purpose of this paper is to present self-consistent simulations performed

with parameters closer to those of the experiments and to make comparison with experimental data for Lundquist numbers up to about 10^7. Our principal finding is that the reduced-MHD simulations reproduce the behavior of small and medium size tokamaks surprisingly well, e.g., with respect to sawtooth period and collapse time. In particular, the collapse time shows a much weaker dependence on resistivity than the $S^{1/2}$ dependence expected from the Sweet-Parker scaling [11,12], mainly because the change in central q over the sawtooth cycle decreases with increasing S. Consequently, the amount of helical flux $\Delta\psi_*$ to be reconnected decreases with resistivity and this partly compensates for the decrease in reconnection rate, $d\psi_*/dt$. Furthermore, in the nonlinear simulations, the maximum growth-rate of the resistive kink mode scales weakly with S, roughly as $S^{-1/3}$. The weak dependence on S results from the modification of the equilibrium profiles by the sawteeth themselves, such that the shear changes from practically zero inside a central region to order unity over one resistive layer width. The sawtooth period shows a weaker than linear dependence on S, in agreement with experimental results.

In carrying out these simulations, we have found that the character of the sawteeth is sensitive to the values of the transport coefficients, in particular to the ratio of the perpendicular viscosity ν to perpendicular heat conductivity $\chi_\perp$. If $\nu/\chi_\perp$ is too small, the characteristic relaxation oscillation of the sawteeth is replaced by more or less continuous mode activity and the equilibrium never departs significantly from marginal stability with q = 1 in a large central region. However, if $\nu/\chi_\perp > 1$, distinct relaxation oscillations are produced. The reason for this dependence is that the viscosity influences the damping rate of the postcursor oscillation. If the damping is weak, the postcursor does not have time to decay before the next crash is triggered, and continuous mode activity results. Recent experimental results concerning momentum confinement from Doublet III [13], TFTR [14] and ASDEX [15] all indicate that the momentum

confinement is of the same order as the energy confinement, although both are anomalous.

2. The model

Our simulations are based on the standard, straight cylinder, low-β, reduced-MHD equations [16]. The code [10] evolves the electron temperature selfconsistently with a highly anisotropic thermal diffusivity and ohmic heating. The perpendicular thermal conductivity has been inferred from temperature measurements on the Frascati Tokamak (FT). In normalized units, the model equations are:

$$
\begin{aligned}
&\left(\frac{\partial}{\partial t} + \underline{v}\cdot\nabla_\perp\right)\omega = \underline{B}\cdot\nabla j + \nu\,\nabla_\perp^2\omega \quad , \\
&\frac{\partial\psi}{\partial t} = \underline{B}\cdot\nabla\phi - \eta\,(j - j_{bs}) + E_z(t) \quad , \\
&\left(\frac{\partial}{\partial t} + \underline{v}\cdot\nabla_\perp\right)T = \frac{2\eta}{3} j\,(j - j_{bs}) \qquad (1) \\
&\qquad + \nabla_\perp\cdot\chi_\perp\nabla_\perp T + (\underline{B}\cdot\nabla)\chi_{\parallel}(\underline{B}\cdot\nabla)T \quad ,
\end{aligned}
$$

where $\underline{B} = \nabla\psi\times\hat{z} + B_T\hat{z}$, ψ is the magnetic flux function, $\underline{v} = \nabla\phi\times\hat{z}$, and ϕ is the stream function, $\omega = -\nabla_\perp^2\phi$ is the vorticity and $j = -\nabla_\perp^2\psi$ is the plasma current. Moreover, j_{bs} is the bootstrap current [17], T is the electron temperature, η is the neoclassical Spitzer resistivity and $\nabla_\perp = \nabla - \hat{z}\,\partial/\partial z$. The unit length is the minor radius a, the unit time is the Alfvén transit time $\tau_A = R/v_A$, where R is the major radius and v_A is the Alfvén speed in the toroidal magnetic field B_T. ν and $\chi_\perp$ are the perpendicular viscosity and perpendicular thermal diffusivity multiplied by τ_A/a^2 and $\chi_{\parallel}$ is the parallel thermal diffusivity multiplied by τ_A/R^2. The temperature corresponds to the poloidal beta of the electrons divided

by q_a^2, $T = (R/a)^2 \beta/2$. In the following we shall refer to this normalized beta as β_{pol}. The normalized temperature is also a measure of the ratio of the energy confinement time, $\tau_E = 3nT/2\eta j^2$ and the resistive diffusion time, $\tau_R = a^2 \mu_0/\eta$.

The code uses finite differences with 200 points in the radial direction and Fourier expansion in the azimuthal and toroidal directions. The present study is restricted to single-helicity perturbations with m/n = 1, and mode number up to m=4 (in some cases m=8) have been retained. The applied toroidal field E_z (t) has been adjusted in time to keep the q-value at the edge fixed. No assumption has been made regarding the symmetry of the perturbations, i.e., ψ, ϕ and T have all been expanded with both cosine and sine components.

We have chosen as a reference case a typical ohmic discharge in FT, with B_T = 6T, a = 0.20 m, R = 0.83 m, q_a = 2.6, central density n(0) ~ 1.8×10^{20} m^{-3} and central temperature T(0) between 500 and 1000 eV. With these parameters, the Alfvén time is $\tau_A \sim 0.085$ μsec, the Lundquist number is $S = \tau_R/\tau_A \sim 10^7$, the normalized parallel thermal conductivity is $\chi_{\parallel} \sim 20$ and the normalized temperature is $T \sim 0.02 \div 0.04$. We have assumed a radial dependence of the type $\chi_\perp(r) = \chi_\perp(0)/[1-(r/r_0)^2]^2$, with $r_0/a = 1.1$, for the perpendicular thermal diffusion coefficient to represent the results of power balance studies on FT. $\chi_{\parallel}$ and ν have been taken constant over the cross-section.

3. Dependence on thermal diffusivity and viscosity

In general terms, the sawtoothing can be thought of as a nonlinear, dissipative system, in which relaxation oscillations occur. As is well known in nonlinear dynamics, the behavior of such systems is often sensitive to the parameter values, in particular to the dissipation coefficients. We have observed that this is indeed the case for the sawteeth: simulations

performed initially with somewhat randomly chosen parameter combinations (η, ν, $\chi_\perp$ and $\chi_{\prime\prime}$) would produce very different results ranging from distinct sawteeth to weak, continuous mode activity. To obtain some understanding of the influence of the parameters on the character of the sawteeth, we first studied the dependence on ν and $\chi_\perp$ at moderate S. We emphasize that the scaling studies presented here are self-consistent, taking full account of modifications in the equilibrium profiles, that result from the action of the sawteeth themselves. Such modifications lead to important and unexpected results for the dependence on the Lundquist number.

Figure 1 shows the time evolution of the central temperature and safety factor and integrated energies W in the Fourier components 1/1 and 4/4 for three different values of β_{pol}: 0.022, 0.15 and 1.35. For all the three cases, $S = 10^4$ and $\nu = 10^{-4}$, and for those with β_{pol}=0.15 and β_{pol}=1.35, we have discarded the trapped particle corrections in the resistivity and bootstrap current. Figure 1 shows clearly that as β_{pol} is reduced by increasing $\chi_\perp$ (i.e., by decreasing the energy confinement time), the period of the sawteeth decreases, and their character of distinct relaxation oscillations is lost. The relaxation oscillations of the 1/1 mode energy are very pronounced in the high-β case, whereas for lower β, where the sawtooth period is shorter, the postcursor of one crash does not have sufficient time to decay before the next crash occurs. The values of $\chi_\perp(0)$ in the three cases of Fig. 1 are 1×10^{-3}, 7×10^{-5} and 7×10^{-6}, which may be compared with the viscosity $\nu = 10^{-4}$. The case of $\beta_{pol} = 1.35$ corresponds closely to that simulated by Denton et al [8]. In this case, the variation in q_0 over the sawtooth cycle is large, $\Delta q_0 \approx 0.25$.

If we try to represent the sawtooth period of these three cases as a power of β_{pol}, i.e., $\tau_{saw} \propto \beta_{pol}^{\alpha_\beta}$, the dependence is rather strong $\alpha_\beta \approx 0.8$. Thus the energy confinement time plays an important role for determining the period of the sawteeth.

In FT, $\beta_{pol} \approx 0.02 \div 0.04$ and the corresponding case in Fig. 1 does not have regular sawteeth. However, the character of the sawteeth is also dependent on the viscosity. Figure 2 shows the time histories of T_0, q_0 and the mode energies for four different values of viscosity, 10^{-3}, 10^{-4}, 10^{-5}, and 10^{-6}. The resistivity η and the perpendicular heat conductivity $\chi_\perp$ are a factor of 20 larger than the reference case, i.e., $S = 5\times10^5$, $\chi_\perp = 2\times10^{-5}$. Whereas distinct relaxation oscillations are produced for $\nu = 10^{-3}$ and 10^{-4}, the activity becomes irregular for $\nu \leq 10^{-5}$, as is most clearly seen from the plot of $q_0(t)$. As ν is decreased, the period of the sawteeth decreases from $\tau_{saw} \approx 3.3\times10^3\ \tau_A$ at $\nu = 10^{-3}$ to $\tau_{saw} \approx 1\times10^3\ \tau_A$ at $\nu = 10^{-6}$. The dependence of the sawtooth period on viscosity is shown in Fig. 3. For $\nu \geq 10^{-5}$, we find $\tau_{saw} \propto \nu^{\alpha_\nu}$ with $\alpha_\nu \approx 0.3$.

The reason for the irregular behavior when $\nu \leq 10^{-5}$, which is similar to the case of small β in Fig. 1, can be understood from the time evolution of the mode energies. The variation in the 1/1 mode energy is close to four orders of magnitude at $\nu = 10^{-3}$ and slightly less than one order of magnitude when $\nu = 10^{-6}$. An important role of the viscosity is to control the decay of the postcursor of the internal disruption by changing both the damping rate and the repetition time. The damping rate of the energy in the 1/1 mode, W_{11}, is about 10×10^{-3} for $\nu = 10^{-3}$ and 5×10^{-3} for $\nu = 10^{-6}$. This dependence is rather weak, but nevertheless has a strong influence on the character of the sawteeth, in particular as the periodicity time also increases with viscosity. We note that when the viscosity is of the same order as the resistivity or larger, it reduces the growth rate of the internal kink mode according to $\gamma \propto (\eta^2/\nu)^{1/3}$ [18], which also tends to make the period increase with ν.

The three parameters $\chi_\perp$, ν and η affect the sawteeth in very different ways. Viscosity increases the damping of the postcursor and slows down the growth of the precursor. As a consequence, increasing ν gives longer sawtooth period and more pronounced relaxation oscillations. Increasing

β_{pol} at fixed η gives longer sawtooth period as the ohmic heating time increases. Since β_{pol} (or $\chi_\perp$) does not much influence the damping of the postcursor, larger β_{pol} also gives more pronounced relaxation oscillations. We note that the experimental relation $\nu \approx \chi_\perp$ lies within, but not far from the boundary of the region that produces sawtooth-like oscillations in Figures 1 and 2.

The influence of resistivity is more complex. At fixed β_{pol} and ν, the repetition time increases with S, but this is partly counterbalanced by a decrease of the damping and growth rates. The former effect is, however, stronger and the net result is more clear relaxation oscillations at large S. This can be seen by comparing Figs. 1a and 2b, where S changes from 1×10^4 to 5×10^5, while β_{pol} and ν are fixed. On the other hand, if ν is scaled in proportion to $\chi_\perp$, as suggested by experiments, the character of the sawteeth at fixed $\beta_{pol} \propto \eta/\chi_\perp$, shows a very weak net dependence on S, as we show in Sect. 4.

In addition to the dependence on β_{pol} and ν discussed here, the sawteeth are sensitive to the parallel thermal conductivity [9,10]. Too small a value of $\chi_{||}$ will completely eliminate the sawteeth, and instead give rise to a steady m=1/n=1 convection pattern, which may be thought of as a nonlinear form of the rippling mode. We have found that the threshold value of $\chi_{||}$ for regular sawteeth to occur is approximately that which makes a temperature perturbation in the $q \approx 1$ region (where the q profile is very flat) decay by one order of magnitude between two successive crashes. The normalized parallel conductivity for FT, obtained from classical transport theory, is about 20, which is sufficient for this condition to be fulfilled in the range of parameters that we have explored. Therefore, we have not further studied the dependence on the parallel thermal conductivity, and used a fixed value of $\chi_{||} = 27$.

4. Dependence on Lundquist number

As shown in Sec. 3, the sawteeth are sensitive to the transport coefficients, $\chi_\perp$, ν and η. It would be desirable to make a complete parameter study (at least three-dimensional) but this would be very costly in computer time. Instead, we have taken the point of view that in comparing tokamaks of different size, the primary variations are those in S, while νS and $\chi_\perp S$ stay relatively constant. We therefore consider the reference parameters for FT quoted in Sec. 2 and scale these by introducing an enhancement factor E for all the small transport coefficients ($\chi_\perp$, ν , and η). We shall show that the often assumed scalings for the growth-rate of the resistive kink mode and the total collapse time are not applicable to the sawteeth because they do not take into account the modifications that occur to the equilibrium profiles as a result of the sawteeth themselves. By means of self-consistent simulations we have found that these modifications are dependent on the S-value. Thus, the scalings with S are strongly affected by this self-consistency, which has hitherto been largely ignored.

In Fig. 4, we show the sawtooth period as a function of S, with νS and $\chi_\perp S$ fixed, for our reduced-MHD simulations together with experimental data points [4,19-24]. To account for of the dependence on β_{pol}, we applied the approximate scaling of Sec. 3, $\tau_{saw} \propto \beta_{pol}^{0.8}\, \nu^{0.3}$ with $\nu \propto \chi_\perp \propto \beta_{pol}^{-1}$. This implies that, for fixed S, the net dependence on β_{pol} is $\tau_{saw} \propto \beta_{pol}^{0.5}$. Therefore, the experimental points have been plotted as $\tau_{saw}/\tau_A \beta_{pol}^{0.5}$. (In comparing data for ohmic discharges, the exponent for β_{pol} is not very sensitive, as β_{pol} does not vary by much between different machines.) The agreement in Fig. 4 is striking; the simulation results fall within the scatter of the experimental data for $S \leq 10^6$, while at $S = 10^7$, the period is somewhat too short, for example, in comparison with FT. It is seen from Fig. 4 that with τ_R/τ_E fixed, $\tau_{saw}/\tau_A \propto S^{\alpha_s}$, with $\alpha_s \approx 0.7$.

We now discuss the results for various enhancement factors E=25, E=5 and E=1 more in detail. Figure 5 shows the time histories of central temperature and safety factor together with the mode energies in the three cases. It is clear from Fig. 5 that the variations in q_0 and T_0 diminish as S increases. For example, at $S = 4 \times 10^5$, $\Delta q_0 \approx 0.05$ and $\Delta T_0/T_0 \approx 40\%$, whereas at $S = 10^7$, $\Delta q_0 \approx 0.009$ and $\Delta T_0/T_0 \approx 15\%$. This is consistent with the fact that τ_{saw} shows a weaker than linear dependence on S.

It has been noted [4] that the collapse time in JET is very short (≤ 500 μsec), and that this seems to be at variance with resistive reconnection rates and also with a resistive mode as trigger for the internal disruption [5]. Instead, ideal instability has been suggested as a likely candidate for the trigger [25,26]. While this conclusion appears well founded for a machine of JET size, where S is between 10^8 and 10^9, we strongly argue that the Kadomtsev-like sawteeth simulated here are in excellent agreement with experimental data for S up to 10^7. In Fig. 6 we show the collapse time (i.e., the time-scale over which T_0 drops) and the growth times of the linear instability, both obtained from the nonlinear simulations, for the three values of E.

Notably, both of these times scale weakly with S and at $S = 10^7$, they are in good agreement with observations on FT. Figure 6 indicates that the linear growth-rate scales approximately as $S^{-1/3}$. This is exactly as would be expected from linear theory, if the shear at the q=1 surface were independent of S. Given that dq_0/dt scales as 1/S and that the resistive kink mode becomes unstable as soon as $q < 1$ anywhere, one might expect that the shear at q=1 during the linear growth phase decreases with increasing S. This reasoning assumes that the q-profile near q=1 is independent of S. However, in comparing the q-profiles in the three cases E=25, 5 and 1, we find that the shear $s = rq'/q$ is <u>not</u> a fixed function of $r - r_{q=1}$. Instead, we find that s varies considerably <u>within one resistive layer width,</u> between practically 0 on the inside to about 0.3 on the outside, even though the

resistive layer shrinks with increasing S. Thus, the current gradients become increasingly steep at the edge of the low-shear region as S increases and the effective shear for the linear instability is approximately independent of S. In Fig. 7 we show the q-profile together with the m=n=0 current profile for E = 5 ($S = 2\times10^6$) at the time of maximum growth-rate for the m=1 component, and during the end of the reconnection phase. The very steep current gradient is built up during the non-linear end phase of the crash (Fig. 7c) just outside the low shear region, where a corresponding jump in the q-profile can also be observed (Fig. 7d). The generation of a negative spike in the current profile at the boundary of the reconnection region was predicted already by Kadomtsev [2]. Furthermore, the q-profile in Fig. 7b is slightly hollow, but not sufficiently to produce double sawteeth [8,27]. However, we find that the tendency to form a hollow q-profile is more pronounced at high S. This tendency is in agreement with experimental observation; double sawteeth occur much more frequently in large machines with $S \geq 10^7$, and only very rarely in a machine of TCA size [24], where S is a few times 10^6.

In order to compare the resistive growth rates with those found in ideal computations [26], we have varied q_{min} for a fixed current profile (Fig. 7a), simply by rescaling the current. The result is shown in Fig. 8. Note that a change of less that 2×10^{-3} in q_{min} produces a growth-rate $\gamma = 10^{-3}\,\tau_A^{-1}$, i.e., the threshold for instability is very steep. (The deviation of the threshold q_{min} from unity is within the numerical error for the radial resolution in our computation.) Figure 8 applies for $S = 2 \times 10^6$. For larger S, the absolute growth-rate of the resistive kink decreases, however, the steepening of the current profile partly compensates, and the growth-rate remains a very steep function of q_{min}. The net dependence of the maximum 1/1 growth rate over the sawtooth cycle in the nonlinear simulations is rather weak, approximately $\propto S^{-1/3}$, as shown in Fig 6.

The collapse time also shows a weak dependence on S, much weaker than the $S^{1/2}$ dependence expected from Sweet-Parker scaling [11,12]. This is easily understood, since, as shown in Fig. 5, the variation in q_0 decreases for increasing S and, therefore, also the amount of helical flux to be reconnected. It is important to realize that the effective Alfvén frequency well inside the low shear region, ($\propto |q_0-1|$), does not necessarily play any role in determining the rate of reconnection, as the rigid m=1 displacement of the interior is not an Alfvén wave but rather the reduced-MHD version of the fast magnetosonic wave. (The fast wave does exist in reduced MHD as a "surface wave", with $\omega = -\nabla_\perp^2\phi = 0$, analogous to pressure perturbations in incompressible fluid mechanics. For the m=1 mode the "surface wave" is a rigid displacement of the core, due to "forces" $\underline{B}\cdot\nabla j$ acting at its boundary.) Thus, the effective ideal time for the nonlinear reconnection is determined by the shear at the the edge of the low-shear region rather then the Alfvén time in the centre. This is in exact analogy with the linear theory.

It is clear from the plots of the mode energies that at the end of the internal disruption, the m=4/n=4 mode is excited to rather high amplitude, and the question arises whether our simulations with $m \leq 4$ have sufficient angular resolution. To check this, we have rerun the case at $S=2\times10^6$ keeping Fourier components up to m=8/n=8. The result for $T_0(t)$ is shown in Fig. 9. When examining gross features, such as $T_0(t)$, the four Fourier components give adequate resolution. However, if we consider details of the evolution, certain differences become apparent, notably the formation of small secondary islands along the q=1 separatrix [28] which are seen with eight modes but not with four. These details appear to have only very slight influence on the gross properties and global evolution. In Fig. 10 we show contour plots of the helical flux function $\psi_* = \psi - (a^2 - r^2)/2$ at various stages of the internal disruption for the eight-mode simulation at $S=2\times10^6$. The formation of the small secondary island is followed by coalescence

with the primary one. Furthermore, components with m>2 are excited at rather high amplitude, as is evident also in the contour plots of the temperature (Fig.11). We note from the temperature plots that the shape of the hot core changes during the internal disruption from a circle to a crescent, as has been observed in JET [29] and TFTR [30].

Another issue of resolution concerns the influence of multiple helicity interactions. For example, the very steep current profile in Fig. 7c would make tearing modes with nearby rational surfaces unstable. This effect was, in fact, predicted on theoretical grounds by Kadomtsev [2], and was observed in a multiple-helicity simulation at moderate S [10], where the m/n = 4/3, 5/4, 6/5, etc. modes where periodically destabilized by the sawteeth. Clearly, this destabilization would be very powerful in the high-S cases as seen from Fig. 7c. Thus, we expect that multiple helicity reconnection must occur during the late phase of the internal disruption, when the current gradient is particularly steep. This will lead to an increase in the reconnected flux, and thus prevent Δq_0 from becoming exceedingly small at large S. The occurrence of multiple helicity interactions in a region just outside the low shear region can also be argued from experimental observations in TFTR [30] concerning the heat pulse generated by the sawtooth crash. Very fast, poloidally asymmetric propagation is observed outside the reconnection radius where n > 2 tearing modes with m/n near unity may have grown to sufficient amplitude to stochasticize the magnetic field. We are planning to address the influence of the multiple helicity interactions in the near future.

5. Scaling of the sawtooth period

Our simulations predict that at fixed q_a, the sawtooth period scales as $\tau_A \beta_{pol}^{0.5} S^{0.7}$, which, as shown in Fig.4, gives a good fit between different machines. To compare with scalings observable in a single machine it is

useful to display the dependence on the plasma parameters: the density n, the temperature T, Z_{eff}, the ratio between the ion mass and the proton mass A, the toroidal field B_T and the linear dimensions. From $\tau_{saw} \propto \tau_A \beta_{pol}^{0.5} S^{0.7}$ we obtain:

$$\tau_{saw} \propto (R/B_T)^{1.3} A^{0.15} a^{0.4} f(Z_{eff})^{-0.7} n^{0.65} T^{1.55} , \qquad (2)$$

where

$$f(Z_{eff}) = Z_{eff} [0.29 + 0.457 / (1.077 + Z_{eff})] \qquad (3)$$

is the Z_{eff} dependence of the resistivity . It should be noted that the scaling (2) has been obtained keeping q_a fixed. When the density is changed at fixed current, the temperature will change, and the relation T=T(n) would allow us to give the absolute dependence of the sawtooth period from the electron density. The scaling (2) is in reasonable agreement with that observed in FT [31], where $\tau_{saw} \propto n^{0.5}$ is observed together with a weak inverse dependence of the temperature on the density. On some machines, TFR [32] and TCA [24], τ_{saw} depends linearly on n, but part of this dependence may be due to changes in the profiles and Z_{eff}.

6. Discussion

We have simulated sawteeth using a reduced-MHD code with transport. In this model, the sawteeth occur via a resistive kink mode and complete resistive reconnection. Our main conclusion is that such a model is in excellent agreement with experimental results, concerning sawtooth period and crash times, for S-values up to about 10^7. We observe that when S increases, certain changes to the equilibria occur, that make the precursor growth time and the nonlinear crash time scale very weakly with S. One effect is the steepening of the current profile at the edge of the low shear region which enhances the linear growth-rate at high S. The other is the

decrease in Δq_0 with increasing S over the sawtooth cycle, which decreases the amount of flux to be reconnected and, hence, makes the crash time of the sawtooth depend very weakly on S. As a result of these changes, the resistive kink mode does give growth-rates and crash times in agreement with experiment for S up to about 10^7. Furhermore, the sawteeth have been found sensitive to the values of the transport coefficients. In particular, the perpendicular viscosity ν must be of the same order as, or larger than, the perpendicular heat diffusivity $\chi_\perp$, for regular sawteeth to occur.

It is quite evident that for $S > 10^7$, the present model would have to be modified. If the scenario presented here is extrapolated to higher S, Δq_0 and the repetition time appear to become too small. In addition, the current profile at the edge of the low shear region would become extremely steep, and multiple helicity interactions must be expected as discussed in Sec. 4. Experimental data from JET [4,33] suggest that at very high S, ideal modes are involved in the trigger [25,34] and presumably also in the subsequent spreading of the hot core [35]. From the theoretical point of view, several effects can be pointed out, that have not been included in the present reduced-MHD computations, but could significantly affect the behavior of the sawteeth. The most obvious of these is, of course, toroidicity and compressibility, which have been studied in recent full MHD computations [26,36]. Furthermore, as the ideal-MHD stability at $q = 1$ is generally speaking close to marginal, it is also clear that many non-MHD effects such as particle drifts and significant populations of hot particles expected in certain RF-heating scenarii and, in future experiments, alpha particles, may be important [37]. In view of several unexpected results from the present reduced-MHD simulations, not to speak of the variety of sawteeth observed experimentally, we are well aware that new surprises may be in store when self-consistent simulations using more complete models are carried out at Lundquist numbers characteristic of large tokamaks.

Acknowledgement

One of the authors (G. Vlad) thanks the Euratom for having provided mobility funds to support his stay at the CRPP where most of this work has been done on the CRAY-1S computer at the EPFL.

References

[1] von GOELER, S., STODIEK, W., SAUTHOFF, N.R., Phys. Rev. Lett. **33** (1974) 1201.

[2] KADOMTSEV, B.B., Fiz. Plasmy **1** (1975) 710 [Sov. J. Plasma Phys. **1** (1975) 389].

[3] SOLTWISH, H., STODIEK, W., MANICKAM, J., SCHLUTER, J., in Plasma Physics and Controlled Nuclear Fusion Research 1986 (Proc. 11th Int. Conf., Kyoto, 1986), IAEA, Vienna (1987), vol 1, 263.

[4] CAMPBELL, D.J., GILL, R.D., GOWERS, C.W., et al., Nucl. Fusion **26** (1986) 1085.

[5] WESSON, J. A., Plasma Phys. Controlled Fusion **28** (1986) 243.

[6] WADDELL, B.V., ROSENBLUTH, M.N., MONTICELLO, D.A., WHITE, R.B., Nucl. Fusion **16** (1976) 528.

[7] SYKES, A., WESSON, J.A., Phys. Rev. Lett. **37** (1976) 140.

[8] DENTON, R.E., DRAKE, J. F., KLEVA, R.G., BOYD, D.A., Phys. Rev. Lett. **56** (1986) 2477.

[9] DENTON, R.E. , DRAKE, J. F., KLEVA, R.G., Phys. Fluids **30** (1987) 1448.

[10] BONDESON, A., Nucl. Fusion **26** (1986) 929.

[11] SWEET, P.A., in Electromagnetic Phenomena in Cosmical Physics (Cambridge U.P., New York, 1958) p 123.

[12] PARKER, E.N., J. Geophys. Res. **62** (1957) 509.

[13] BURRELL, K.H., GROEBNER, R.J., St. JOHN, H., SERAYDARIAN, R.P. , Nucl. Fusion **28** (1988) 3.

[14] SCOTT, S.D., FONCK, R.J., BITTER M., et al., in Controlled Fusion and Plasma Physics (Proc. 15th Eur. Conf. Dubrovnik 1988) Vol 12B, Part I, European Physical Society (1988), 103.

[15] ROBERTS, D.E., MAYER, H.M., FUSSMAN, G., et al., in Controlled Fusion and Plasma Physics (Proc. 15th Eur. Conf. Dubrovnik 1988) Vol 12B, Part I, European Physical Society (1988), 15.

[16] STRAUSS, H.R., Phys. Fluids **19** (1976) 134.

[17] HINTON, F.L. HAZELTINE, R.D., Rev. Mod. Phys. **48** (1976) 239

[18] PORCELLI, F., Phys. Fluids **30** (1987) 1734.

[19] MCGUIRE, K., ROBINSON, D. C., Nucl. Fusion **19** (1979) 505.

[20] ALLADIO, F., BARDOTTI, G., BARTIROMO, R., et al., in Controlled Fusion and Plasma Physics (Proc. 14th Eur. Conf. Madrid 1987) Vol 11D, Part I, European Physical Society (1987), 73.

[21] RIEDEL, K.S., EBERHAGEN, A., GRUBER, O., et al., Nucl. Fusion **28** (1988) 1509.

[22] FREDRICKSON, E.D., CALLEN, J.D., MCGUIRE, K., et al., Nucl. Fusion **26** (1986) 849.

[23] KNOWLTON, S., PORKOLAB, M., TAKANASE, Y., MIT report PFC/JA 87.32 (1987).

[24] SIMM, C.W., Ph.D. thesis , Ecole Polytechnique Fédérale de Lausanne (1987) [LRP 334/87].

[25] WESSON, J.A., KIRBY, P., NAVE, M.F.F., in Plasma Physics and Controlled Nuclear Fusion Research 1986 (Proc. 11th Conf., Kyoto, 1986), IAEA, Vienna (1987), vol 1, 3.

[26] HASTIE, R.J., HENDER, T.C., CARRERAS, B.A., CHARLTON, L.A., HOLMES, J.A., Phys. Fluids **30** (1987) 1756.

[27] PFEIFFER, W., Nucl. Fusion **25** (1985) 673.

[28] BISKAMP, D., Phys. Fluids **29** (1986) 1520.

[29] GRANETZ, R.S., SMEULDERS, P., Nucl. Fusion **28** (1988) 457.

[30] MCGUIRE, K.M., ARUNSALAM, V., BARNES, C.W., et al., Plasma Phys. Controlled Fusion (to appear 1989).

[31] ALLADIO, F., BARDOTTI, G., BARTIROMO, R., et al., in Controlled Fusion and Plasma Physics (Proc. 14th Eur. Conf. Madrid 1987) Vol 11D, Part I, European Physical Society (1987), 77; and ALLADIO, F., private communication (1988).

[32] TFR GROUP, in Plasma Physics and Controlled Nuclear Fusion Research 1976 (Proc. 6th Int. Conf., Berchtesgaden, 1976), IAEA, Vienna (1977), vol 1, 279.

[33] DUPERREX, P.A., POCHELON, A., EDWARDS , A., et al., in Controlled Fusion and Plasma Physics (Proc. 15th Eur. Conf. Dubrovnik 1988) Vol 12B, Part I, European Physical Society (1988), 362.

[34] AYDEMIR, A.Y., Phys. Rev. Lett. **59** (1987) 649.

[35] BUSSAC, M.N., PELLAT, R., in Theory of Fusion Plasmas, Proc. Workshop, Varenna, 1987 (Editrici Compositori, Bologna, 1988).

[36] AYDEMIR, A.Y., et al., in Plasma Physics and Controlled Nuclear Fusion Research 1988 (Proc. 12th Int. Conf., Nice, 1988), IAEA (to appear 1989).

[37] WHITE, R.B., RUTHERFORD, P.H., COLESTOCK, P., BUSSAC, M.N., Phys. Rev. Lett. **60** (1988) 2038.

Figure captions

Figure 1. Time evolution of the central temperature T_o, safety factor in the center q_o and integrated energies W in the Fourier components m/n=1/1 and m/n=4/4 for three different values of the poloidal beta : a) $\beta_{pol} \approx 0.022$, b) $\beta_{pol} \approx 0.15$, c) $\beta_{pol} \approx 1.35$. $S=10^4$ and $\nu=10^{-4}$. The unit time is the Alfvén transit time τ_A.

Figure 2. Time evolution of the central temperature T_o, safety factor in the center q_o and integrated energies W in the 1/1 and 4/4 Fourier components for four different values of the viscosity: a) $\nu=10^{-3}$, b) $\nu=10^{-4}$, c) $\nu=10^{-5}$, d) $\nu=10^{-6}$. $S=5\cdot10^5$ and $\beta_{pol} \approx 0.02$.

Figure 3. Sawtooth period τ_{saw}/τ_A versus viscosity ν for $S=5\cdot10^5$ and $\beta_{pol} \approx 0.02$.

Figure 4. Normalized sawtooth period $\tau_{saw}/\tau_A \, \beta_{pol}^{0.5}$ versus Lundquist number S: black circles are the simulation results obtained for $\beta_{pol} \approx 0.02$ varying S while keeping νS and $\chi_\perp S$ fixed ($\nu S \approx 24$ and $\chi_\perp S \approx 10$). Other symbols refer to typical shots for different tokamaks.

Figure 5. Time evolution of the central temperature T_o, safety factor in the center q_o and integrated energies W in the 1/1 and 4/4 Fourier components for three different values of the Lundquist number $S=10^7/E$ with E=25,E=5,E=1. The other parameters are the same of Fig.4.

Figure 6. Growth time of the linear instability (open circles) and collapse times of the central temperature (crosses; for each value of S are shown the minimum and maximum value observed among several teeth). The other parameters are the same of Fig.5.

Figure 7. a) Current density profile j(r) (m=n=0) and b) safety factor profile q(r) (only in the central region of the plasma) for the case of Fig.5, $S=2 \cdot 10^6$, at the time of maximum growth rate ($t/\tau_A=20720$); c) current density profile and d) safety factor profile during the nonlinear phase ($t/\tau_A=22020$).

Figure 8. Linear growth rate (in τ_A^{-1}unit) as the minimum of the safety factor q_{min} is varied (rescaling the current) for the current profile shown in Fig.7a.

Figure 9. Time evolution of the central temperature T_o and mode energies W for the last crash of Fig. 5 ($S=2 \cdot 10^6$): a) and b) simulation with Fourier components up to m/n=4/4 ; c) and d) simulation with Fourier components up to m/n=8/8.

Figure 10. Contour plots of the helical flux function for the eight-mode simulation in Fig. 9 ($S=2 \cdot 10^6$). Contours are plotted only in the region of low shear.

Figure 11. Contour plots of the temperature for the eight-mode simulation of Fig. 9 ($S=2 \cdot 10^6$).

FIG. 1

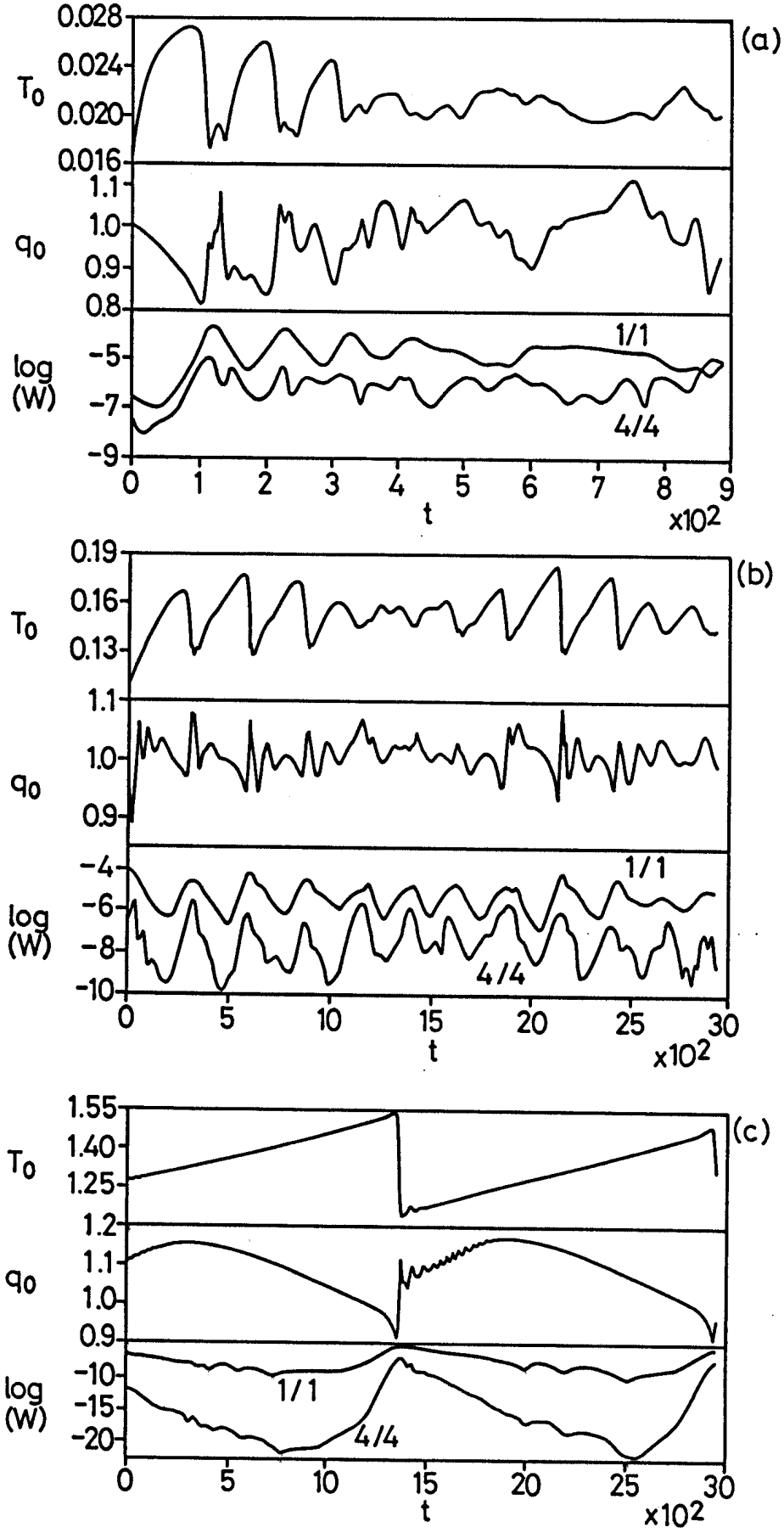
(a)
T_0
0.028
0.024
0.020
0.016
q_0
1.1
1.0
0.9
0.8
log (W)
-5
-7
-9
1/1
4/4
0 1 2 3 4 5 6 7 8 9
t
x10²
(b)
T_0
0.19
0.16
0.13
q_0
1.1
1.0
0.9
log (W)
-4
-6
-8
-10
1/1
4/4
0 5 10 15 20 25 30
t
x10²
(c)
T_0
1.55
1.40
1.25
q_0
1.2
1.1
1.0
0.9
log (W)
-10
-15
-20
1/1
4/4
0 5 10 15 20 25 30
t
x10²

FIG. 2

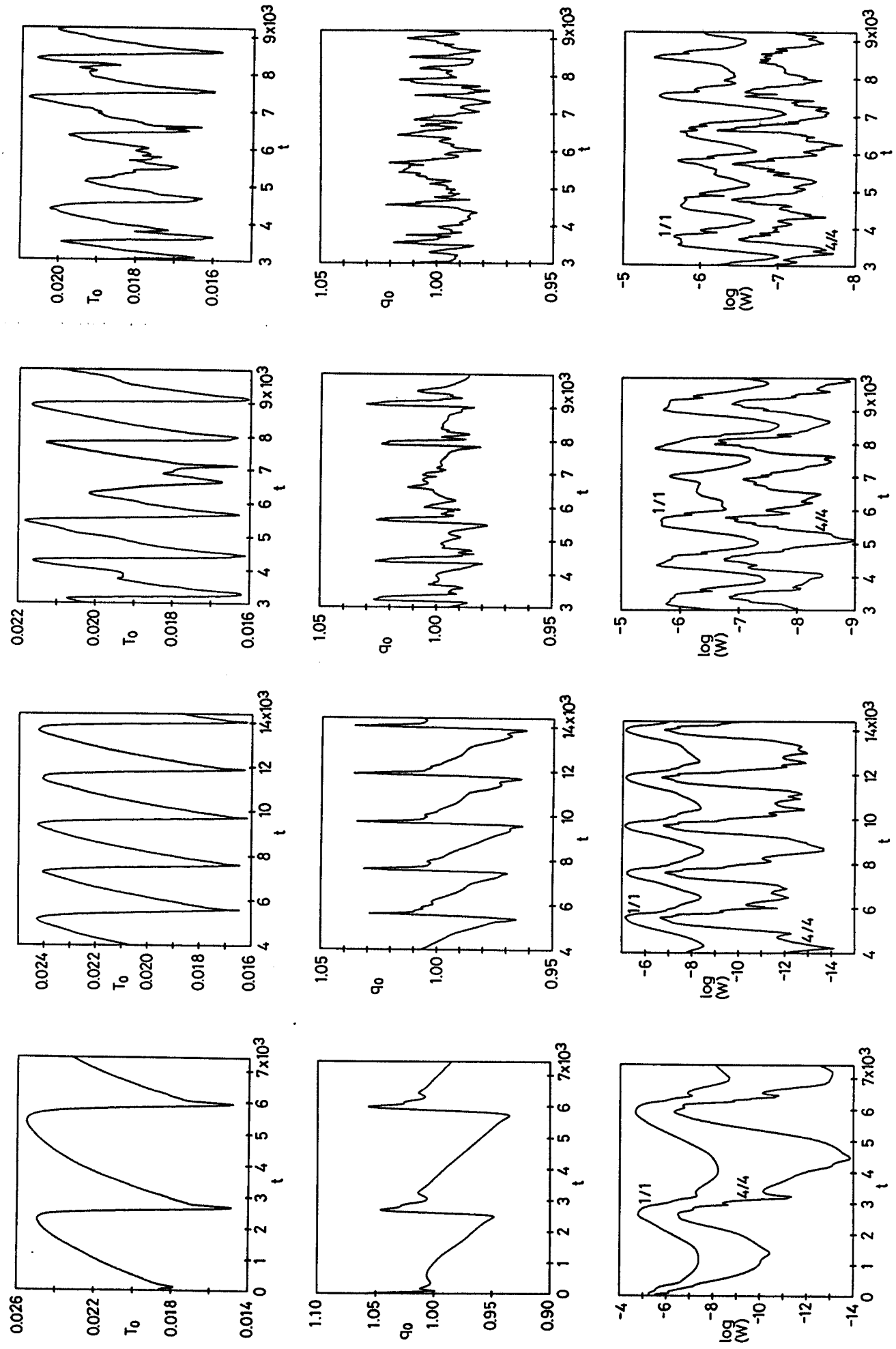

FIG. 3

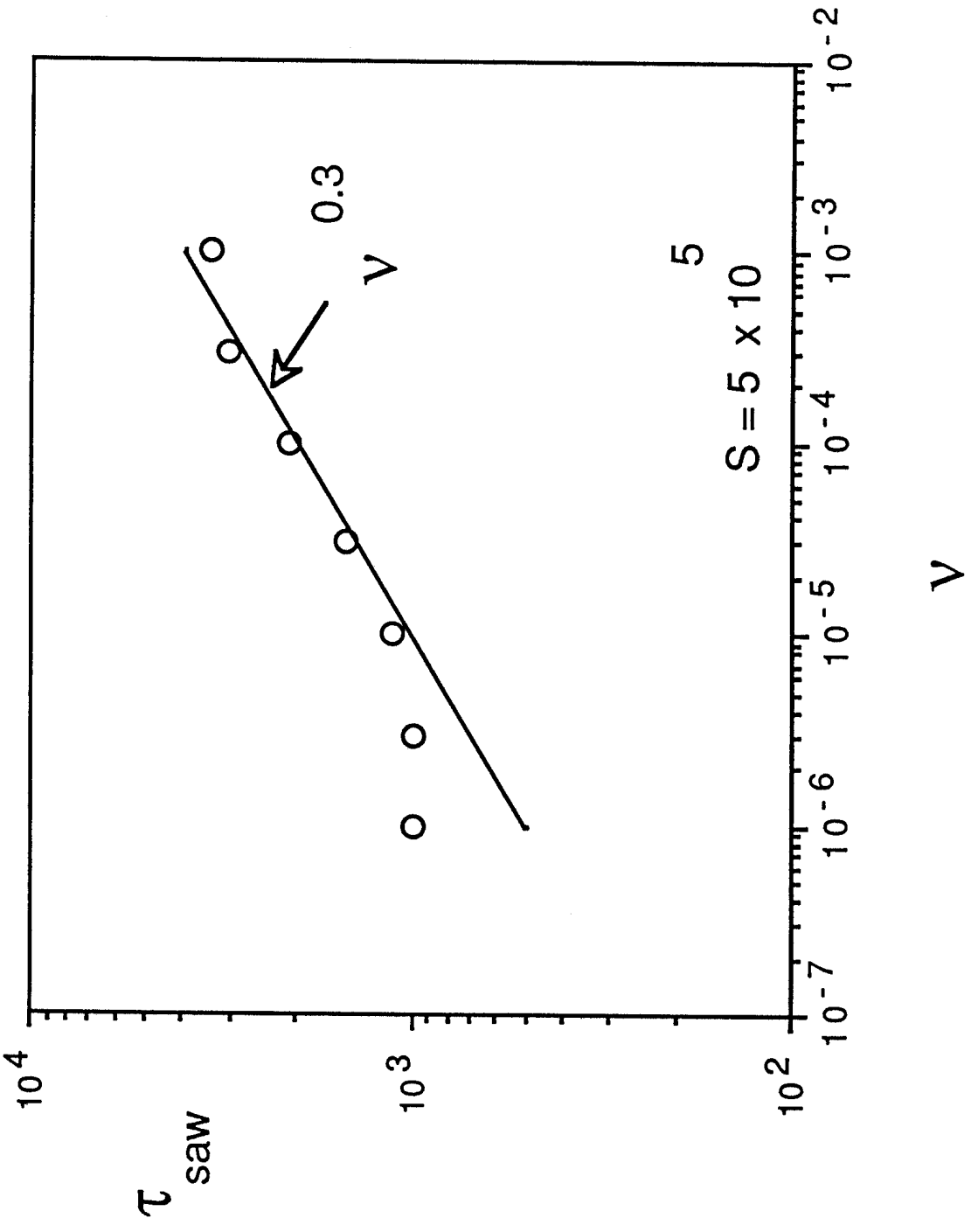

FIG. 4

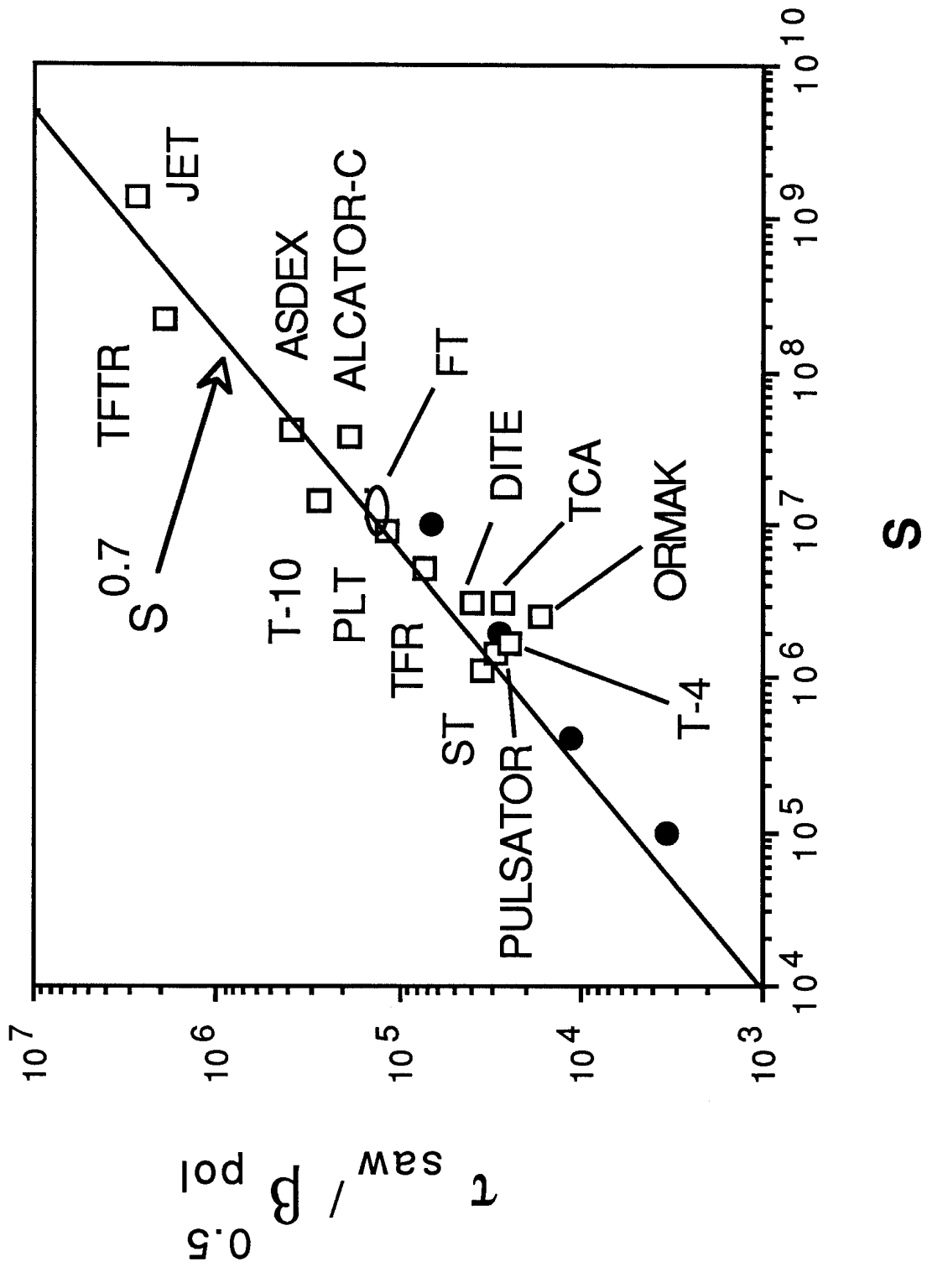
$\tau_{saw} / \beta_{pol}^{0.5}$
S
10^3
10^4
10^5
10^6
10^7
10^4
10^5
10^6
10^7
10^8
10^9
10^{10}
$S^{0.7}$
TFTR
JET
ASDEX
ALCATOR-C
FT
DITE
TCA
ORMAK
T-10
PLT
TFR
ST
PULSATOR
T-4

FIG. 5

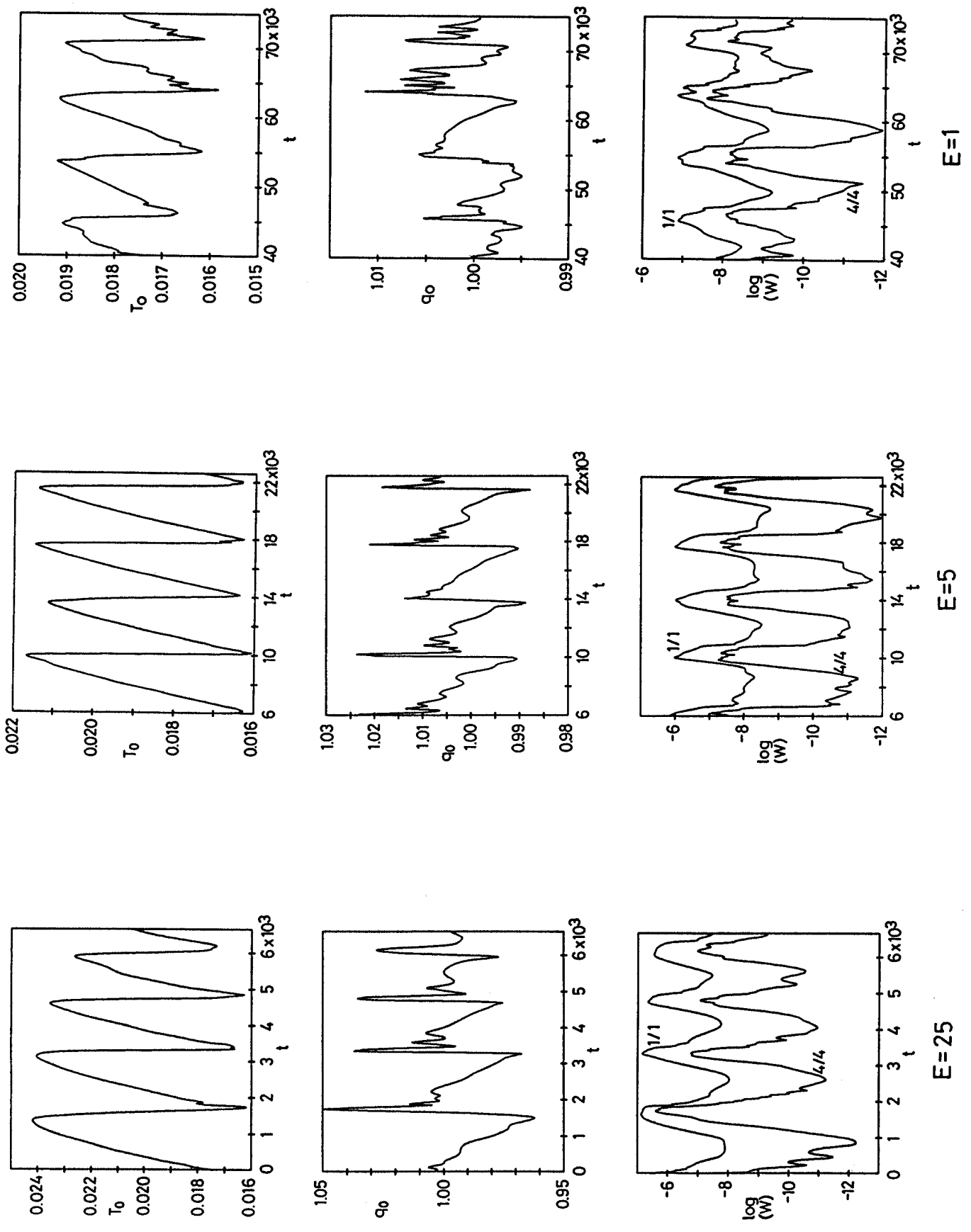
E=25
E=5
E=1
T_0
q_0
log (W)
1/1
4/4
t
0.024
0.022
0.020
0.018
0.016
1.05
1.00
0.95
-6
-8
-10
-12
0
1
2
3
4
5
6x10³
6
10
14
18
22x10³
0.022
0.020
0.018
0.016
1.03
1.02
1.01
1.00
0.99
0.98
40
50
60
70x10³
0.020
0.019
0.018
0.017
0.016
0.015
1.01
1.00
0.99

FIG. 6

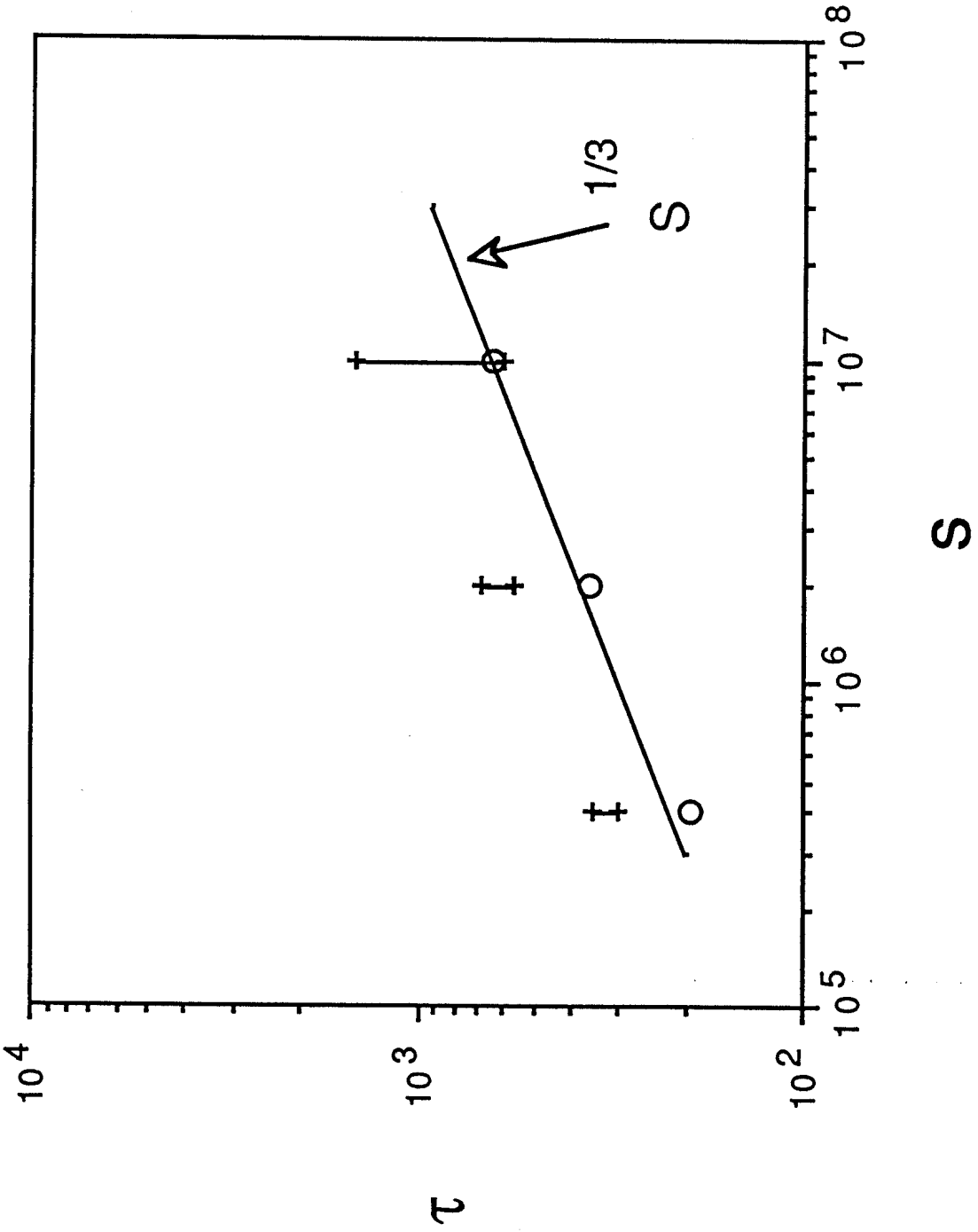

FIG. 7

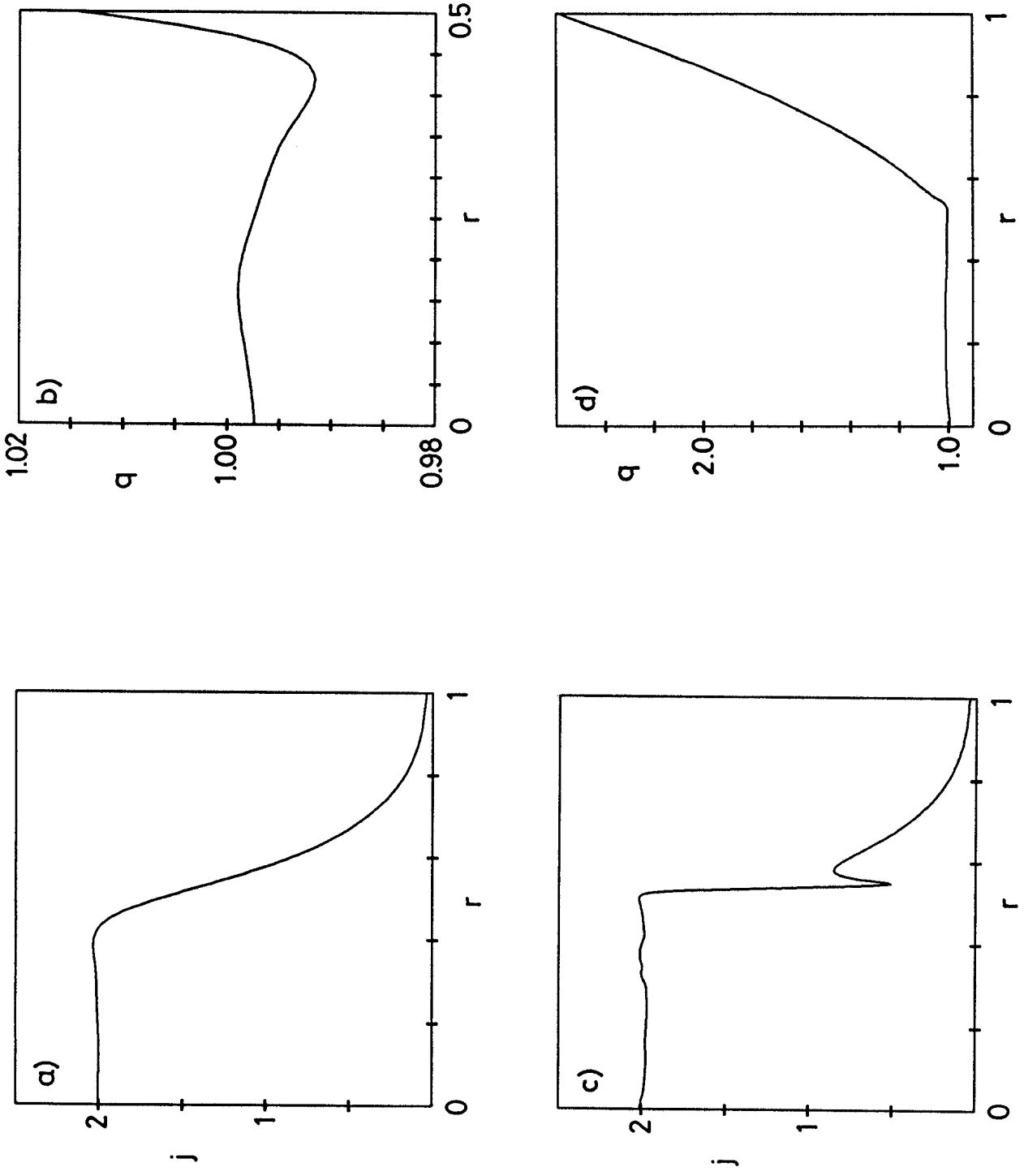

FIG. 8

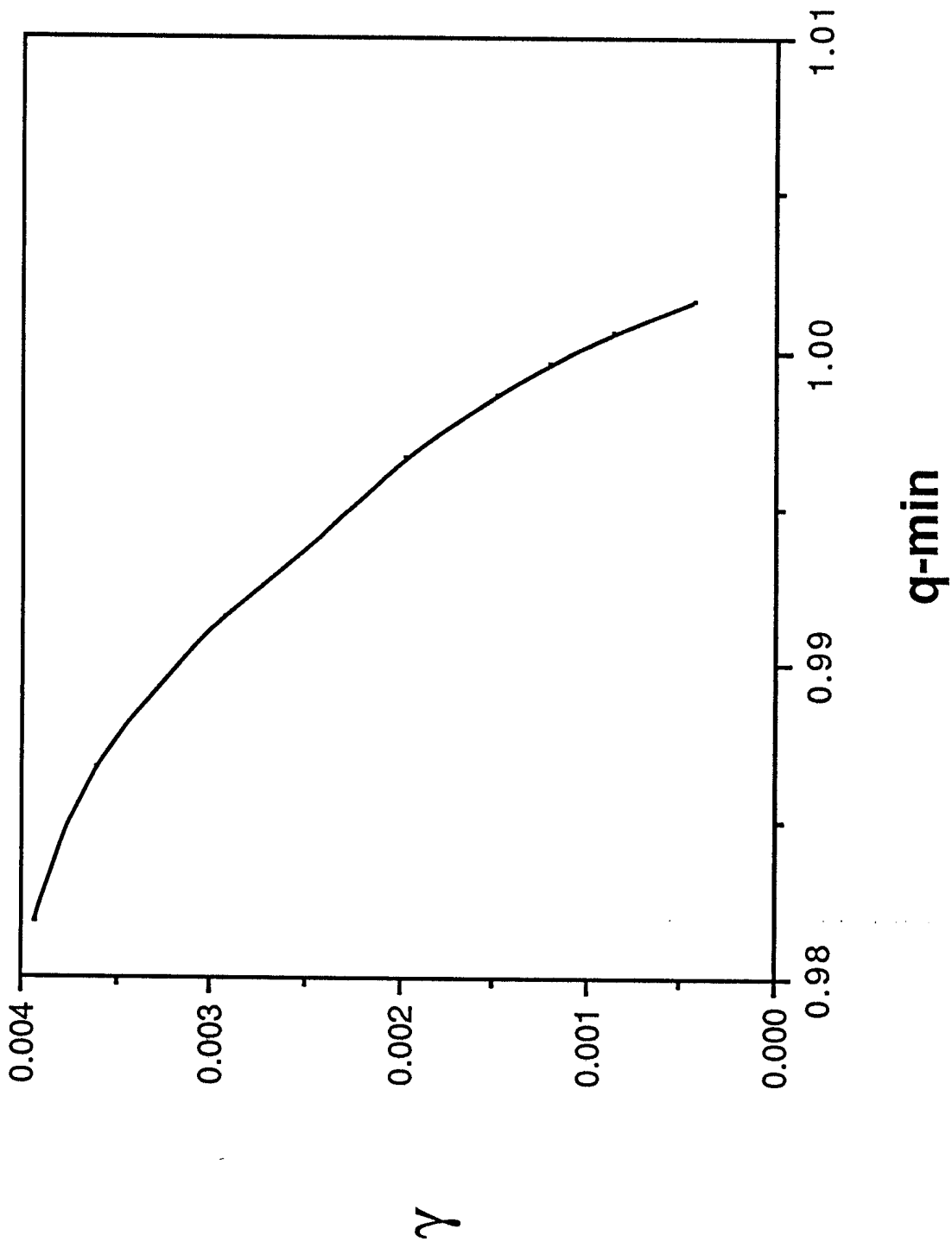

FIG. 9

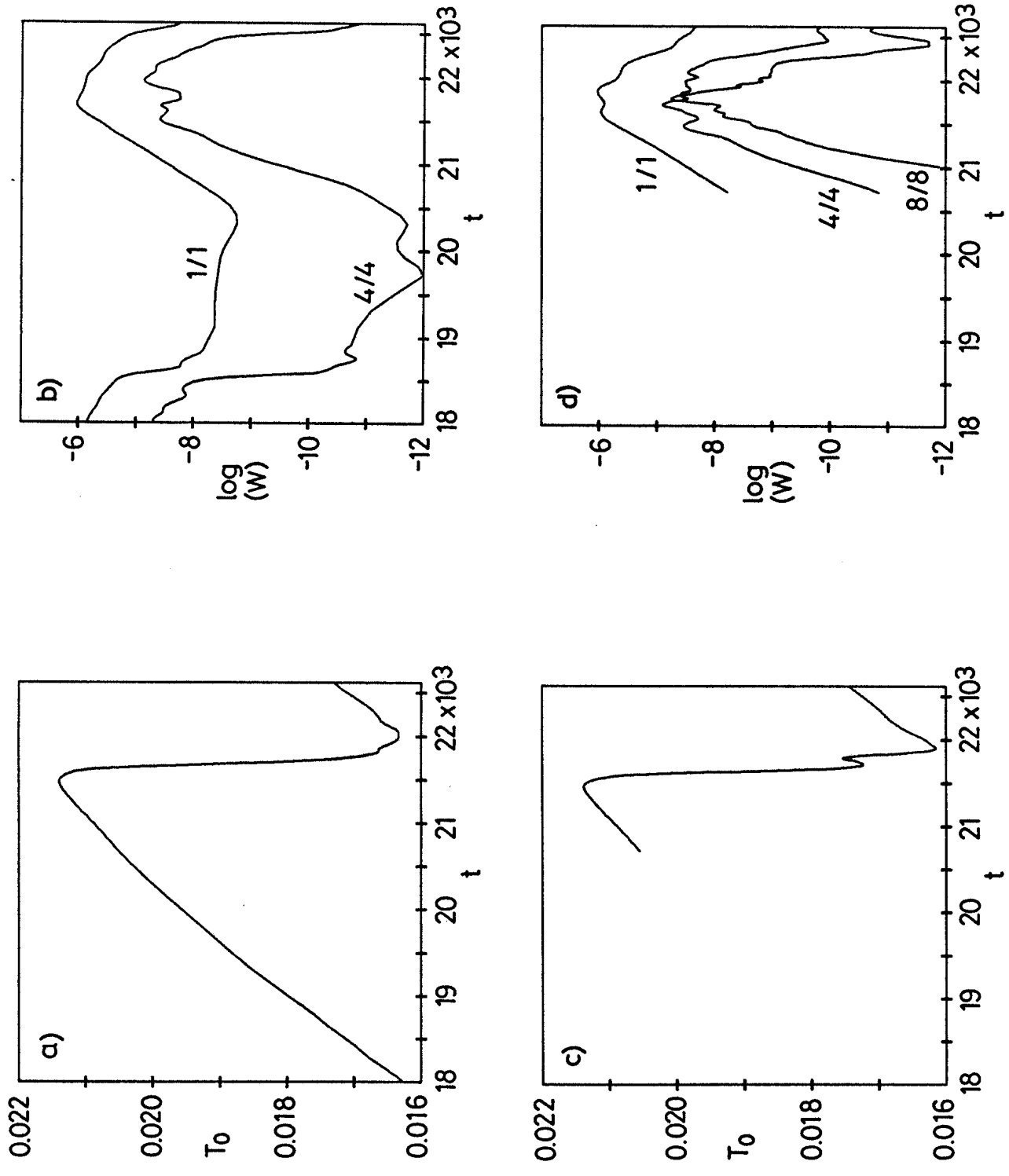
a)
b)
c)
d)
0.022
0.020
0.018
0.016
T_0
18
19
20
21
22 x103
t
-6
-8
-10
-12
log (W)
1/1
4/4
8/8

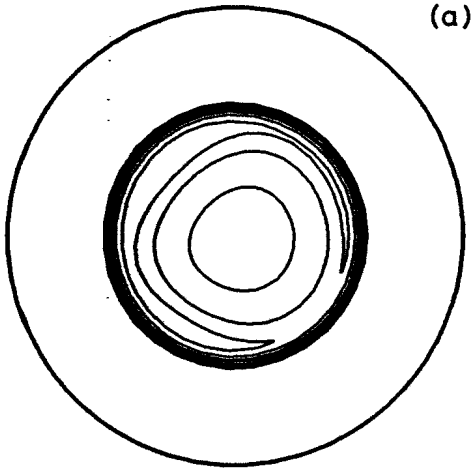

t = 21220 ; ψ_{min} = - 0.13971,
ψ_{max} = - 0.13718;

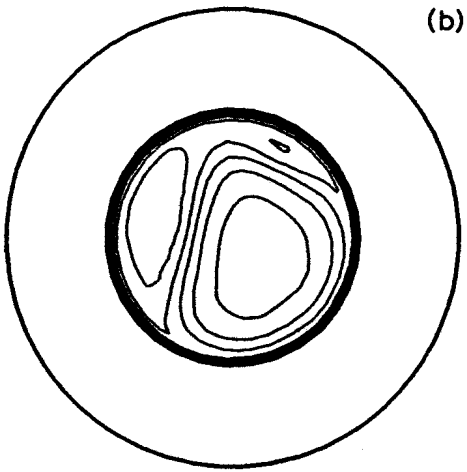

t = 21520 ; ψ_{min} = - 0.13986,
ψ_{max} = - 0.13812;

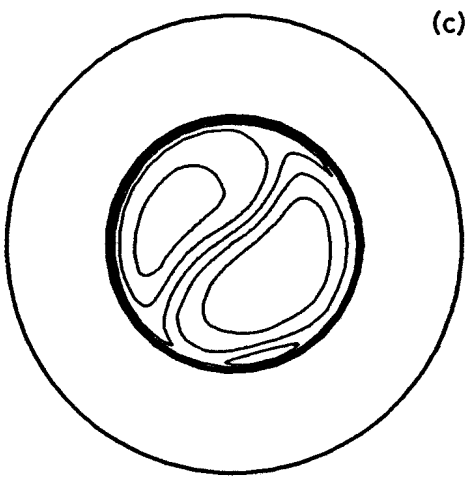

t = 21620 ; ψ_{min} = - 0.13987,
ψ_{max} = - 0.13812;

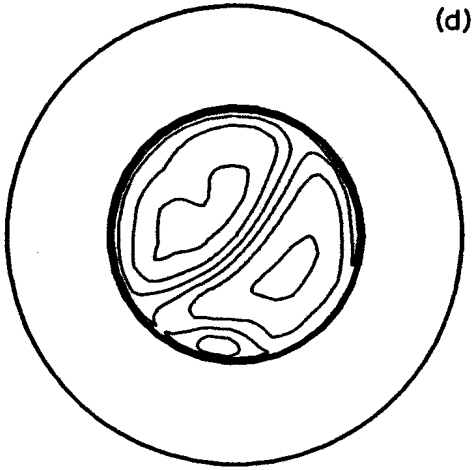

t = 21720 ; ψ_{min} = - 0.13991,
ψ_{max} = - 0.13813;

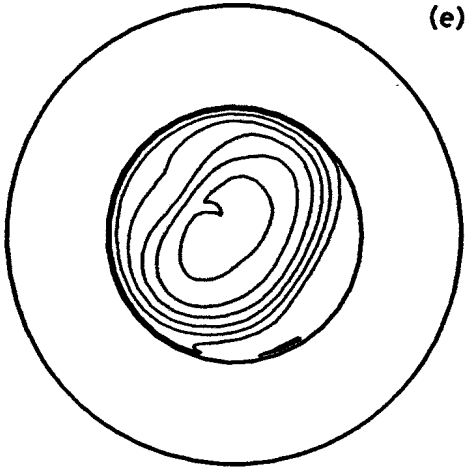

t = 22020 ; ψ_{min} = - 0.13989,
ψ_{max} = - 0.13813.

FIG. 10

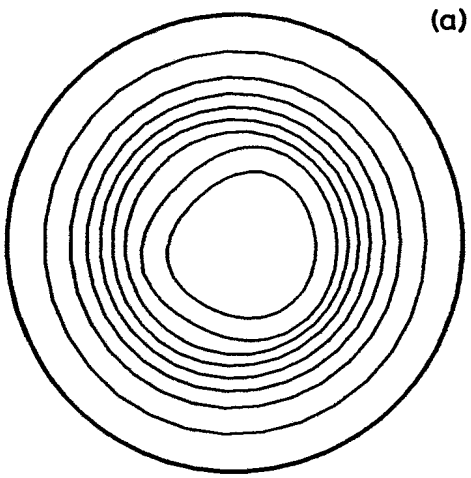

t = 21220 ; $T_{min} = 2.481 \cdot 10^{-3}$,
$T_{max} = 2.001 \cdot 10^{-2}$;

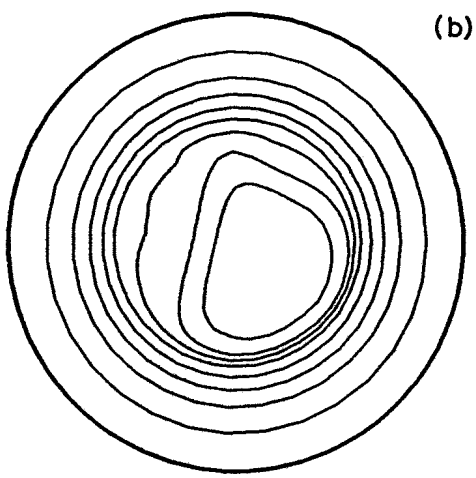

t = 21520 ; $T_{min} = 2.503 \cdot 10^{-3}$,
$T_{max} = 2.034 \cdot 10^{-2}$;

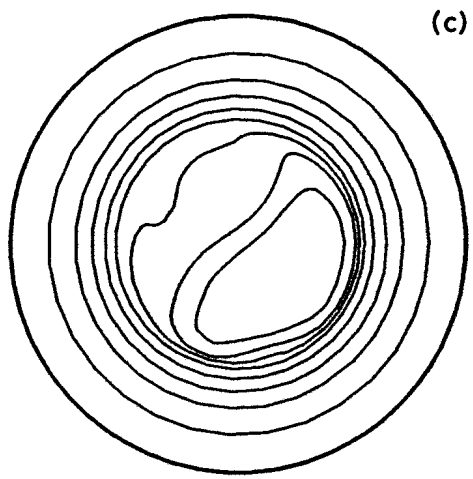

t = 21620 ; $T_{min} = 2.511 \cdot 10^{-3}$,
$T_{max} = 2.046 \cdot 10^{-2}$;

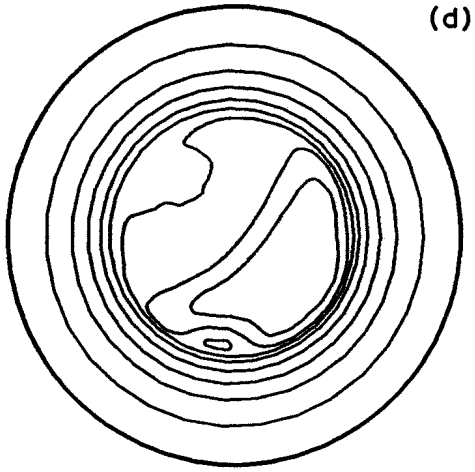

t = 21720 ; $T_{min} = 2.521 \cdot 10^{-3}$,
$T_{max} = 2.062 \cdot 10^{-2}$;

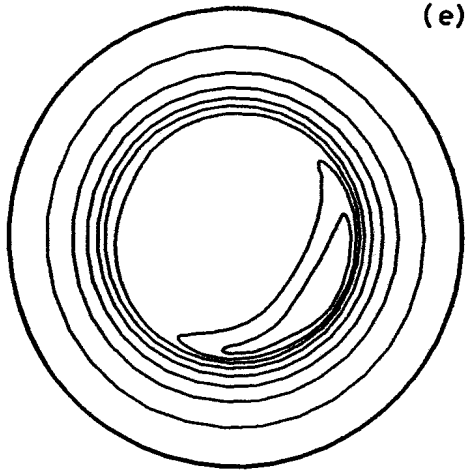

t = 22020 ; $T_{min} = 2.530 \cdot 10^{-3}$,
$T_{max} = 2.074 \cdot 10^{-2}$.

Fig. 11